Monte Carlo Methods for Including Calibration Uncertainties in Model Fitting Analyses

Jeremy J. Drake[a], Peter Ratzlaff[a], Vinay Kashyap[a] and the Chandra MC Uncertainties Team

[a]Smithsonian Astrophysical Observatory, Cambridge MA 02138

SUMMARY

- Instrument response uncertainties are complex and *correlated*, and almost universally ignored in astrophysical X-ray data analyses. For good quality observations, instrument response can be dominant source of error.
- We have developed Monte Carlo methods to treat calibration uncertainties for the *Chandra* ACIS. Here we calcu
- Code and ancilliary data will be released to *Chandra Users*. CIAO *Sherpa* methods are also under development to utilise these techniques (see accompanying poster by Kashyap et al).

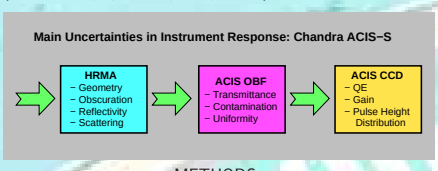

METHODS

Construct different realisations of instrument response by a combination of (1) randomly varying input parameters describing subassembly performance and (2) random multiplicative *perturbation functions*, $\mu(E)$, designed to sample subassembly responses with their assessed uncertainties (Fig. 1). Adopt "curtailed Gaussian" probability distribution $P(\sigma)$ for Monte Carlo draws (Fig. 1a). The different subassemblies were treated as follows:

HRMA On-Axis: Combination of perturbation functions, $\mu_H(E)$, and raytrace-derived effective areas sampling the effects of different hydrocarbon contamination layers and interpretations of XRCF measurements (Figs. 2,3,4).

HRMA Vignetting Function: For off-axis angle θ (in arcmin), include fractional uncertainty of vignetting function, $\bar{V}(\theta)$, and Debye-Waller related function:
$\mu_v(E,\theta) = P(\sigma_v)(1-\bar{V}(\theta)) + \theta P(\sigma_s)(1-R_{DW}/R)$; $\sigma_v, \sigma_s = 0.2$.

ACIS OBF and Contamination Layer: OBF uses perturbation functions, $\mu_{OBF}(E)$, constrained by different allowed maximum deviations and relative edge discontinuities. The contamination perturbation function is:
$\mu_{CL}(E) = e^{-P(\sigma_C)\tau_C + P(\sigma_O)\tau_O + P(\sigma_F)\tau_F + P(\sigma_{FI})\tau_{FI}}$; $\mu_{CL}(0.7keV) < 0.05$
where σ_C, σ_O, σ_F and σ_{FI} are the fractional uncertainties in the optical depths C, O, F and Fluffium at a fiducial date (2003.29).

ACIS QE: combination of perturbation functions, $\mu_{QE}(E)$ and ACIS QE model predictions for uncertainties of 13% in CCD depletion depth and 20% in SiO_2 thickness.

ACIS Gain and Pulse Height Distribution: Uses RMFs generated for $P(\sigma_G)$ variations in gain and pulse height width; σ_G =1% @0.7 keV, 0.5% @1.5 keV, and 0.2% @$\geq$ 4 keV.

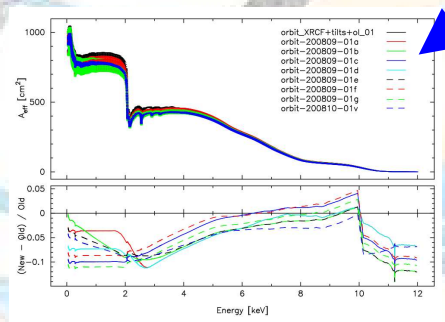

Figure 3. Trial HRMA effective areas that represent the some of the uncertainties in in its calibration. These models were sampled at random as part of the Monte Carlo process, with relative discrete probabilities of 1 for model F (current CALDB model) 0.5 for models A-E and G, and 0.25 for model V.

ESTIMATING EFECTS OF CALIBRATION UNCERTAINTIES

Perturb nominal effective area, and RMF, then use XSPEC to find best-fit model parameters for synthetic *Chandra* ACIS observation computed using the nominal instrument response. Compare with parameters found from fits to 1000 synthetic spectra differing only by Poisson noise and generated using the nominal area and RMF (Figs. 5 and 6). Blackbody, optically-thin thermal plasma, and power law continuum models investigated. **Repeat 1000 times.**

- Limiting accuracy of *Chandra* ACIS reached in spectra with $\sim 10^4$ counts. Beyond this, errors in in best-fit parameters due to calibration uncertainties completely dominate those due to photon noise.

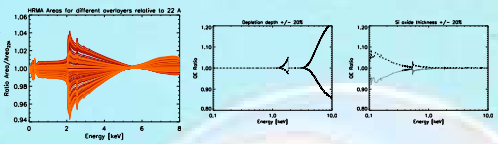

Figure 2. Left: Illustration of the relative change in the HRMA effective area caused by different hydrocarbon contamination layers. The range shown corresponds to the nominal adopted 22$\pm$6 Å layer thickness. **Middle:** Relative changes in the model ACIS S3 QE caused by $\pm$20% differences in the model CCD depletion depth (note that $\pm$13 % was adopted here, which corresponds to a range of about $\pm$10% in the QE at 10 keV). **Right:** QE changes caused by the adopted $\pm$20% differences in CCD SiO_2 thickness.

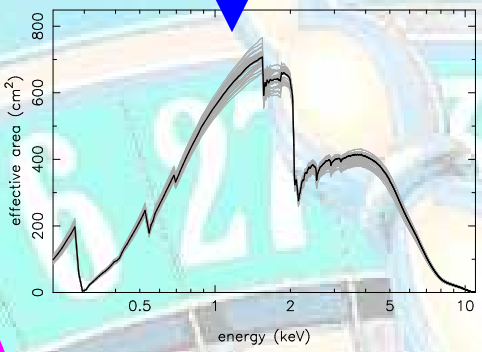

Figure 4. The nominal "seed" *Chandra* ACIS-S effective area (black) compared with a sample of 30 effective areas generated using the Monte Carlo modification method described in the text (grey).

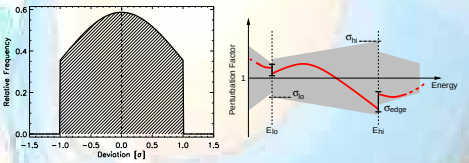

Figure 1. Left: Truncated normal distribution (product of a Gaussian with variance σ^2 and a rectangular Step function with unit density between $\pm\sigma$), $P(\sigma)$, representing the distribution of calibration uncertainties used in the perturbation function and Monte Carlo draws. **Right:** Illustration of a *perturbation function* segment used to apply random deviations from a nominal subassembly response within a given energy range. Within each energy range, E_{lo}–E_{hi}, a random low-order polynomial ($\leq$ 3) is generated that is constrained to lie within the grey shaded region defined by the uncertainties σ_{lo} and σ_{hi}, and also to join up with neighbouring segments within the edge constraints σ_{edge}. The deviation from unity for a large sample of vectors corresponds to $P(\sigma)$.

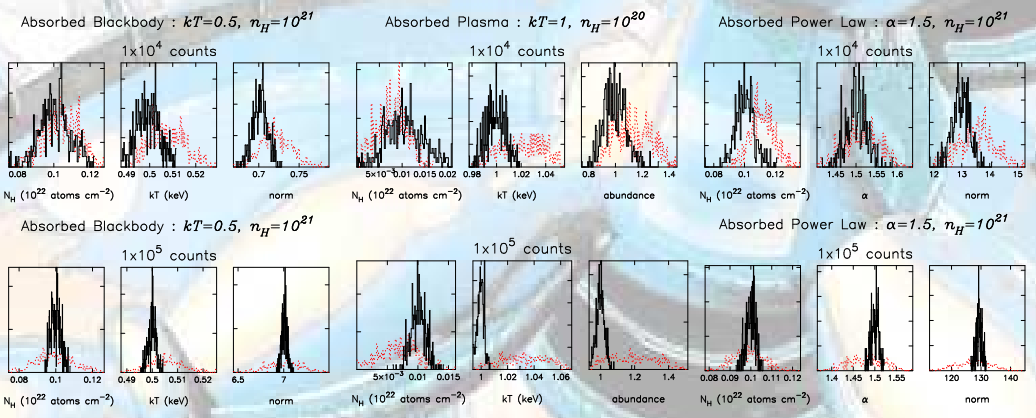

Figure 5. Statistical (black) vs Systematic (red) uncertainties. Example frequency distributions of best-fit parameters obtained for typical blackbody, thermal plasma and powerlaw models from XSPEC for synthetic data sets containing 10^4 (upper panels) and 10^5 (lower panels). Black histograms are distributions resulting from 1000 Monte Carlo samplings of the synthetic data allowing Poisson noise variations alone. Red histograms are the distributions of parameters resulting from fits to a single synthetic data set using 1000 Monte Carlo-generated effective areas and response matrices.

Figure 6. Statistical (black) and Systematic (red) uncertainties comparison. Uncertainty on the best-fit blackbody temperature, thermal plasma temperature and power-law slope as a function of total simulated source counts. Systematic errors begin to exceed statistical errors for sources with $\sim$ 10,000 counts and more. **The limiting accuracy of *Chandra* is reached with 2,000-10,000 counts; increasing an exposure to obtain more than 10,000 counts does not increase the accuracy of the experiment.**